# GEOCHEMICAL PROCESSES AFFECTING GROUNDWATER QUALITY IN WADI SIDRI BASIN, SOUTH SINAI, EGYPT

**Ezzeldin, Hesham A.**
Department of Hydrogeochemistry, Desert Research Center, El-Matareya, Cairo, Egypt
E-mail: h.ezzeldin@drc.gov.eg or h.ezzeldin@hotmail.com

The chemistry of groundwater in arid and semi-arid environments is typically influenced by a set of physical and hydrogeochemical processes that are commonly observed, including precipitation, interaction between water and rocks, and evaporation. It is important to accurately assess the amount and quality of groundwater recharge, as it affects domestic and agricultural activities. This study used traditional diagrams and correlation analysis to understand the hydrochemical processes in the Wadi Sidri basin, Sinai of Egypt and develops a method to estimate rainfall recharge. The trilinear diagram showed that Na and Ca predominate over Mg and K, while strong acids ($SO_4$ + Cl) predominate over weak acids ($CO_3$ + $HCO_3$). The Gibbs plot revealed that rock-water interaction is the primary factor influencing groundwater chemistry. The ion correlations between multiple selected ion ratios, including (Na/Cl)─(Ca/Mg), (Mg/Ca+Mg)─($HCO_3/SiO_2$), ($HCO_3$+$SO_4$)─(Ca+Mg), and (Ca/Ca+$SO_4$)─(Na/Na+Cl) indicated that additional mechanisms, such as reverse ion exchange, direct ion exchange, as well as silicate and carbonate weathering and leaching of interbedded marine deposits influenced groundwater chemistry. The chemical activity diagram revealed that cation exchange processes involving an increase in Na at the expense of Mg control the cation chemistry of groundwater. This diagram, together with the saturation indices obtained by the PHREEQC program, indicated that groundwater is in equilibrium with kaolinite and gibbsite, but is only partially equilibrated with illite. The chloride mass balance method (CMB) was used to estimate the net groundwater recharge by rainfall. It was found that the overall estimate of the recharge for the whole areas was1.78 mm/y for 1981 to 2021 period with a total percentage of the fallen precipitation of 8.06%.

**Keywords**: groundwater, chemistry, recharge, CMB, Wadi Sidri, Sinai

## INTRODUCTION

Mountains, which make up about one quarter of the earth's total land mass, receive an excess quantity of precipitation compared to lowland areas. Runoff of rainfall in the mountains and groundwater withdrawal give an essential water supply to the adjacent lowland areas, that are frequently arid or semi-arid environments (Kapos et al., 2000). As the climate becomes more arid, direct recharge of rainfall into underground aquifers may become less frequent and more unpredictable. This is due to the variations in time of precipitation and climate, as well as the regional variation of outcropping and subsurface rocks, as well as land use (Lerner, 2020).

Groundwater supplies in developing nations, particularly in desert valleys, typically consist of a large number of hand-dug wells that are frequently constructed without proper planning, providing meagre and typically unmonitored water supplies (Hiscock, 2005). Water resources in South Sinai of Egypt are primarily confined to rain and flood waters, which are considered the main source of groundwater recharge, as is the case in many desert areas around the world.

The study area, represented by Wadi Sidri basin, is in Sinai Peninsula and receives a significant amount of rainfall on its mountaintops each year, the majority of which flows as surface runoff into the Gulf of Suez. The remainder evaporates or moves downward via pores or fractures in order to nourish the various wells spread out along the Wadi (Aggour and Gomaa, 2008). The groundwater in Wadi Sidri is an important source of water for the local communities and is used for drinking, irrigation, and other purposes. The sporadic nature of rainfall in the area has resulted in the development of unique ecosystems that are adapted to the arid conditions. The valley provides water for Bedouin settlements that are located nearby. In recent years, the government has initiated several water-harvesting projects to utilize the potential of the area's hydrological resources.

However, due to the arid climate and limited rainfall in the region, the groundwater reserves in this Wadi are under threat of deterioration and depletion. Therefore, proper management as well as conservation of this resource is necessary for the long-term sustainability of the area. Additionally, the chemistry of groundwater in such aquifers is influenced by the composition of the rock formations, hydrogeological conditions, and the presence of anthropogenic activities in the vicinity. These factors highly impact the groundwater chemistry, especially when the sources of the replenishment are becoming more scarce.

There were very limited previous hydrogeochemical investigations conducted in Wadi Sidri (Aggour and Gomaa, 2008 and Afandy et al., 2016). These studies discussed the chemical characterization of groundwater in the light of major ion chemistry and some trace elements, as well as evaluated its quality for irrigation and different agriculture proposes. Other studies

discussed the hydrometeorological hazards and groundwater potential mapping in some basins, including Wadi Sidri basin in Southern Sinai (Masoud, 2011, Elewa and Qaddah, 2011 and Arnous and Omar, 2018). These studies indicated that different geographic locations have varying potential for groundwater storage, but overall, the potential is moderate. Wadi Sidri basin was identified among the basins with high/moderate groundwater potential, which could significantly contribute to sustainable aquifer management. Enhanced groundwater storage is suggested as the best way to sustain water resources as it involves filtering surface water and reduces losses from evaporation and natural catastrophes.

A better understanding of the processes affecting water quality is essential in locating and sustaining usable water supplies. In order to adapt to future changes in groundwater quality, there is need to understand what processes are governing the current spatial variation in groundwater chemistry. Furthermore, it is crucial to identify groundwater recharge sources and to quantify these sources.

In this context, the hydrogeochemical characterization of groundwater reported in this study involve delineating the chemical composition of groundwater, including its mineral content and concentration of ions and some environmental isotopes, to understand the quality and suitability of the water for various purposes. Additionally, a chemical method, the chloride mass balance method (CMB) adopted by Eriksson (1976), is used to estimate recharge rates in the studied aquifers. The use of chloride as an environmental tracer is a widely employed method to estimate the long-term average recharge rates in various groundwater systems, as first proposed by Eriksson and Khunakasem (1969). This method has been applied in diverse environments, including sedimentary aquifers, e.g. studies conducted by Allison and Hughes (1978) and Foster et al. (1982), fractured basement aquifers as discussed by Cook (2003) and regions with both wet and dry climates as demonstrated in studies by Edmunds and Gaye (1994) and De Vries and Simmers (2002).

The study area consists of mountainous terrain with bedrock, sandstone, and limestone formations, as well as valley bottoms covered by thick alluvial sediments. To enhance the conceptual and quantitative understanding of recharge in this complex system, the chloride method was employed. This approach enables the investigation of recharge mechanisms from both the upland bedrock areas and the valley bottom areas via precipitation. The choice of the Eriksson method depended mainly on the available data, which were constrained here by the chloride concentrations in rainwater and groundwater as well as by the annual mean precipitation (mm/y) within a specific period. Afterwards, the recharge estimation results were compared with the other hydrological methods employed in the literature to check the accuracy of the applied method. By using hydrogeochemical characterization and groundwater recharge estimation together, policymakers

and resource managers can make informed decisions about the optimal use of water resources and take steps to mitigate any adverse effects on the environment.

**Study Area**

The study area is situated in the middle part of South Sinai, between 28°47’25’’ and 29°2’40’’latitudes and 33°9’50’’and 33°48’00’’ longitudes covering an area of approximately 1075 km$^2$. Wadi Sidri basin is a significant potential source of enhanced recharge for the aquifer systems of Sinai. Therefore, it was imperative to collect the excess runoff water from this promising drainage basin using commonly used structures such as percolation tanks, check dams, subsurface dams, and injection wells (Elewa and Qaddah, 2011).

Geomorphologically, Wadi Sidri is a steep and narrow valley with an intricate network of tributaries and stream channels, formed by the erosive forces of water over millions of years (Saad et al., 1980). The study area can be classified into three primary units: watershed areas, water collectors, and coastal plain (Fig. 1).

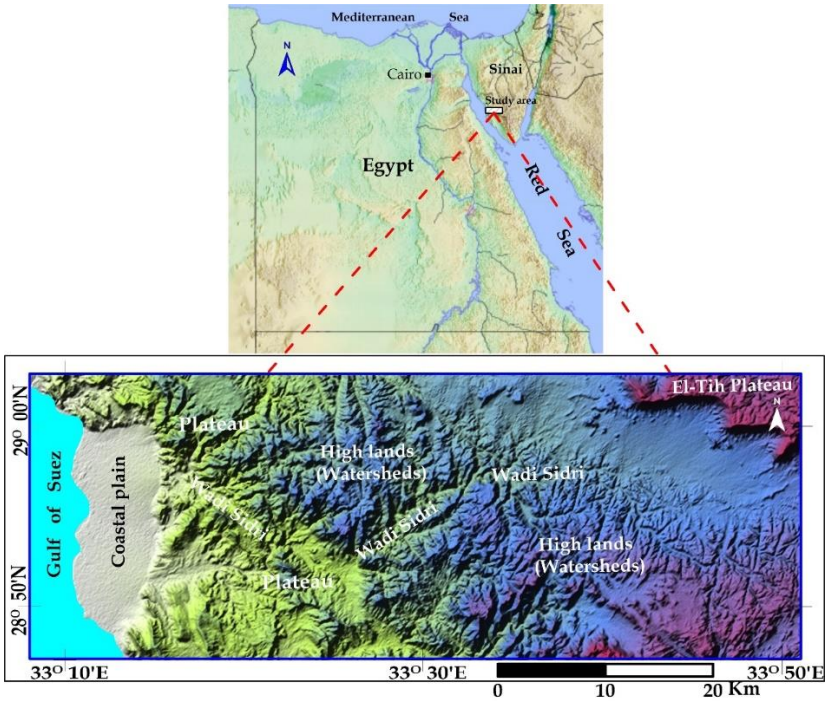


**Fig. (1).** Study area showing the main geomorphologic features (USGS, 2019).

i- The watershed areas (also referred to as highlands) are composed of high mountainous terrain, igneous and metamorphic rocks, and with an

elevation of approximately 1056 meters above mean sea level (amsl). The El-Tih limestone plateau, which surrounds the study area to the east and has an average altitude of 1100 m (amsl), slopes towards the north and northwest, and receives rainwater that is discharged westward to the Gulf of Suez via the drainage network of Wadi Sidri (El Aref, 1988).

ii-The drainage basins, also known as water collectors, are covered by the weathering products of the watersheds, primarily consisting of sands and gravels.

iii- Lastly, the coastal plain is located between the hilly area to the east and the Gulf of Suez to the west, with an average width of 8 km and length of 18.5 km. It is a low-lying area covered by sands and gravels that result from the erosion of the country rocks, including igneous, metamorphic, sandstone, and limestone (Aggour and Gomaa, 2008).

Numerous authors, including Shata (1955), Hammad and Misak (1985), Aglan (1995) and Aggour and Gomaa (2008), have conducted geological studies on South Sinai. The oldest rocks exposed in the region are the Precambrian basement rocks, which are followed by a thick layer of sedimentary rocks ranging in age from the Paleozoic to the Quaternary period.

In the Sidri basin, the fractured Precambrian rocks from the Late Proterozoic period are visible as watersheds. Carboniferous sandstone unconformably overlies the basement rocks, representing the Paleozoic rocks. The Cenozoic rocks consist of Miocene rocks overlying the Upper Eocene, found in the lower portion of Wadi Sidri. Finally, the recent deposits in the area are the alluvial wadi deposits, which are made up of calcareous and ferruginous sandstone mixed with gravel from igneous and metamorphic rock fragments, embedded in a fine matrix of sand and clay (Fig. 2).

Hydrogeologically, groundwater is exploited from the alluvium, carboniferous and weathered basement aquifers.

i- The Quaternary alluvial aquifer: These deposits represent the weathering product of the country rocks of the catchments. They consist of sand and gravels with boulders and cobbles made up of basement rocks, limestone and sandstone (Aggour and Gomaa, 2008). This aquifer is represented by 10 water points (wells 1─10). The groundwater occurs under unconfined condition. The depth to water ranges between 23 m (well no. 12) and 29 m (well no. 14).

ii- The Carboniferous sandstone aquifer: It was tapped by 8 samples (wells 11 ─ 18) in the catchment area. The groundwater in this aquifer exists under unconfined condition at depths varying from 30 m (well no. 16) to 50 m (wells no. 11 and 14).

iii- Fractured Precambrian basement aquifer: Which is considered as the main water bearing formation, was tapped by 12 samples (wells 19 ─ 30). The groundwater in this aquifer exists at depths ranging from 25 m (well no. 20) to 49 m (well no. 29). The hydrogeologic sketch (Fig. 3) illustrates the

subsurface succession of the different water bearing formations in the study area.

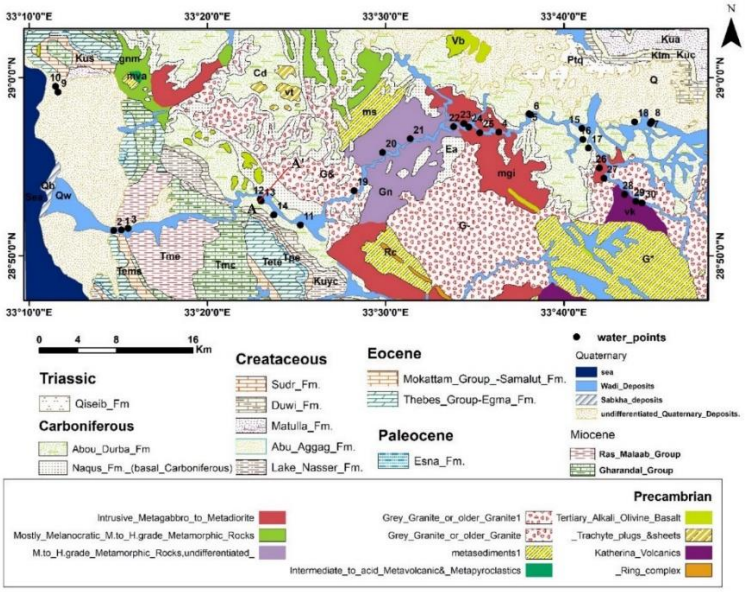


**Fig. (2).** Map showing the outcropping rocks and well locations (CONOCO, 1987).

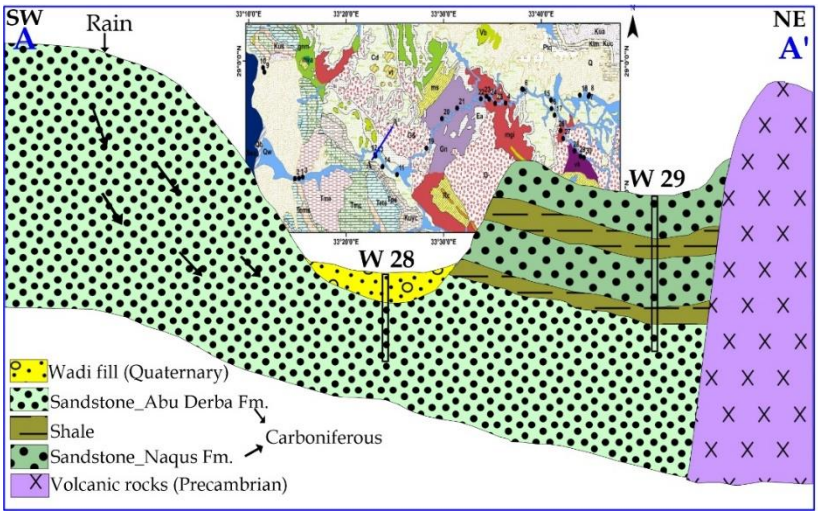


**Fig. (3).** Hydrogeologic sketch showing the groundwater occurrence at Abu Ghraed wells at Wadi Sidri (Aggour and Gomaa, 2008).
*W28 and W29 were wells used by Aggour and Gomaa (2008) to construct this cross-section.

## MATERIALS AND METHODS

This research involves a combination of field measurements, laboratory analysis, and office work. In February 2023, a total of 27 samples were collected, including 6 from alluvium Quaternary, 10 from fractured basements, and 4 from carboniferous sandstone. During the field campaign, measurements such as depth to water, pH, and electrical conductivity were taken. In the laboratory, major ions such as Ca, Mg, Na, $CO_3$, $HCO_3$, $SO_4$, and Cl, as well as minor and trace elements like $SiO_2$, Sr, Al, Fe, Mn, and Zn were analyzed. Major ions were analyzed using the titrimetric (for $CO_3$ and $HCO_3$) and instrumental using the ion chromatography, Dionex ICS-1100 Reagent-Free IC System, for the rest major ions. The charge balance verification of the major ionic constituents was within the limit value of ±5%.

The minor and trace elements were estimated instrumentally using plasma optical emission mass spectrometer (ICP) (POEMSIII, thermo Jarrell elemental company USA). These chemical analyses were performed according to the techniques described in Fishman and Friedman (1989) and Rice et al. (2012). Stable isotopes analysis, including O-18 and deuterium, was conducted using a Picarro L2130-I isotope analyzer with a guaranteed precision of 0.025/0.1. Moreover, the instrument's drift over a 24-hour period is also guaranteed to be minimal, at 0.2/0.8. All the aforementioned analyses were performed at the laboratories of the Desert Research Center of Egypt. The obtained chemical data were then analyzed using conventional techniques such as graphical methods and scatter plots, as well as advanced techniques such as GIS, geochemical modeling, and multivariate statistical analysis.

Furthermore, the CMB was applied to calculate the average annual recharge, which assumes that only precipitation is a source of chloride ions in the groundwater without any contribution from weathering. The recharge rate is proportional to the ratio of chloride concentration in rainfall to that in groundwater, as shown in the following general equation developed by Eriksson and Khunakasem (1969):

$$Recharge\ rate\ (mm) = \frac{rainfall\ (mm)\ \times\ Cl\ concentration\ in\ rainfall\ (mg/l)}{Cl\ concentration\ in\ groundwater\ (mg/l)} \quad (1)$$

The average of the annual precipitation on the study area for the period (1981-2021) were obtained from the website: https://power.larc.nasa.gov/data-access-viewer.

## RESULTS AND DISCUSSION

### 1. The hydrogeochemical Processes and Quality Assessment

### 1.1. Groundwater chemistry and ion ratio relationships

The results of chemical analyses and field measurements for the collected groundwater samples are summarized in Table (1). The results show that the total dissolved solids (TDS) of the alluvium Quaternary aquifer ranged from 1261 to 3069 mg/l, with a mean value of 1819 mg/l; for the Carboniferous sandstone aquifer, the range was from 580 to 3191, with an average of 1519 mg/l; and the values varied from 533 to 2639 mg/l, with an average of 1534 mg/l, for the fractured basement groundwaters. Generally, the TDS of studied groundwater samples ranged from 533 mg/l and 3069 mg/l with an average of 1625 mg/l, reflecting fresh to brackish water types.

The mean TDS value of alluvium was higher than that of carboniferous and weathered basement aquifers. This difference can be attributed to the amount of surface water inflow in the area, as alluvial basins are usually found with large surface water inflow, which leads to a proportional increase in the levels of dissolved minerals as the water percolates into the aquifer. Carboniferous and weathered basement aquifers, however, are in areas with less surface water flow and less permeable rock formations, leading to lower dissolved mineral levels. However, it is worth noting that there can be significant variability in TDS values within each type of aquifer, depending on factors such as the specific location, geological conditions, and the different geochemical processes.

The average pH levels for the alluvium, carboniferous and fractured basement aquifers were 7.32, 7.34 and 6.97, respectively. These pH levels are considered moderate and suggest that there is an equilibrium between the production of $H^+$ ions from weak acid dissociation and the use of hydrogen ions and carbon dioxide through weathering processes, including the conversion of feldspars to kaolinite (Langmuir, 1997). The average values of the calculated total hardness (TH) were 811, 753 and 773 mg/l (as $CaCO_3$), for the alluvium, carboniferous and fractured basement aquifers, respectively. According to the USGS classification of the TH, all the studied groundwater samples are very hard water (TH > 180 mg/l).

Chemical equilibrium speciation and water type calculations were made using Aquachem 10.0 (Waterloo Hydrogeologic, Inc.). In terms of ion dominance and hydrochemical types, groundwater from the Quaternary, Carboniferous sandstone, and fractured basement aquifers showed the same trend and compatibility. This shows that the recharge source for all aquifers is primarily precipitation. The results reveal that Na and Ca were the most dominant cations, followed by Mg and K. The $SO_4$ ion dominates the anions, followed by Cl then $HCO_3$. The groundwater of the three differentiated aquifers reveals two major water types (Table 1), which are dominated by the

**Table (1).** Chemical and isotopic analysis data of the studied groundwater samples.

| ID | Aquifer | EC | pH | TDS | Water type | Ca (ppm) | Mg (ppm) | Na (ppm) | K (ppm) | $CO_3$ (ppm) | $HCO_3$ (ppm) | $SO_4$ (ppm) | Cl (ppm) | $SiO_2$ (ppm) | $\delta^{18}O$‰ | $\delta D$‰ |
|---|---|---|---|---|---|---|---|---|---|---|---|---|---|---|---|---|
| 1 | Q | 2840 | 7.43 | 1836 | Na-Ca-Cl-SO4 | 192.00 | 109.65 | 255.00 | 21.00 | 0.0 | 108.500 | 690 | 514.17 | 6.93 | | |
| 2 | Q | 3350 | 7.45 | 2069 | Na-Mg-SO4-Cl | 205.00 | 137.37 | 278.00 | 24.00 | 0.0 | 114.550 | 840 | 527.58 | 9.12 | -2.85 | -12.82 |
| 3 | Q | 2725 | 6.95 | 1635 | Na-Ca-Cl-SO4 | 185.00 | 84.65 | 245.00 | 19.00 | 0.0 | 98.250 | 560 | 492.24 | 7.00 | | |
| 4 | Q | 2630 | 7.19 | 1763 | Ca-Na-SO4-Cl | 223.08 | 80.88 | 245.00 | 6.50 | 0.0 | 118.035 | 717 | 431.20 | 10.31 | | |
| 5 | Q | 3140 | 7.12 | 2047 | Na-Ca-SO4-Cl | 241.20 | 83.15 | 291.00 | 6.60 | 0.0 | 104.310 | 884 | 489.00 | 9.09 | -3.40 | -15.82 |
| 6 | Q | 2150 | 7.93 | 1406 | Na-Ca-SO4-Cl | 166.12 | 52.44 | 239.33 | 6.40 | 0.0 | 112.545 | 525 | 361.00 | 8.41 | | |
| 7 | Q | 2470 | 7.22 | 1537 | Ca-Na-SO4-Cl | 212.60 | 69.08 | 200.00 | 6.50 | 0.0 | 87.840 | 681 | 323.40 | 3.54 | | |
| 8 | Q | 1980 | 7.27 | 1261 | Na-Ca-SO4-Cl | 152.60 | 41.16 | 206.00 | 5.00 | 0.0 | 109.800 | 473 | 328.30 | 4.30 | -3.80 | -20.17 |
| 9 | Q | 2300 | 7.35 | 1567 | Na-SO4-Cl | 138.84 | 46.24 | 292.00 | 16.20 | 2.7 | 126.270 | 670 | 338.10 | 7.86 | | |
| 10 | Q | 4950 | 7.25 | 3069 | Na-SO4-Cl | 216.60 | 96.07 | 652.00 | 30.20 | 5.4 | 60.390 | 1279 | 759.50 | 5.37 | 4.32 | 28.27 |
| 11 | CSS | 1780 | 7.50 | 1080 | Na-Ca-Cl-SO4 | 124.68 | 35.26 | 181.33 | 7.80 | 0.0 | 101.565 | 362 | 318.10 | 5.91 | -4.28 | -17.96 |
| 12 | CSS | 2220 | 7.27 | 1474 | Na-Ca-SO4-Cl | 155.16 | 53.75 | 239.33 | 8.80 | 0.0 | 115.290 | 587 | 372.40 | 5.24 | | |
| 13 | CSS | 1870 | 6.75 | 1112 | Na-Ca-Cl-SO4 | 116.77 | 42.10 | 193.33 | 8.10 | 0.0 | 118.035 | 394 | 298.90 | 4.14 | -4.05 | -18.82 |
| 14 | CSS | 971 | 7.16 | 580 | Ca-Na-SO4-Cl | 82.36 | 27.95 | 71.60 | 8.90 | 0.0 | 109.800 | 217 | 117.60 | 6.23 | -3.98 | -16.70 |
| 15 | CSS | 5300 | 7.28 | 3191 | Ca-Na-Cl-SO4 | 479.68 | 151.56 | 354.00 | 5.90 | 0.0 | 137.250 | 863 | 1268.00 | 11.55 | -3.28 | -15.95 |
| 16 | CSS | 2770 | 7.79 | 1680 | Ca-Na-Cl-SO4 | 257.52 | 61.75 | 247.00 | 3.80 | 0.0 | 129.015 | 457 | 588.00 | 12.42 | | |
| 17 | CSS | 2120 | 7.81 | 1337 | Na-Ca-Cl-SO4 | 151.08 | 36.74 | 242.00 | 4.10 | 0.0 | 148.230 | 427 | 401.80 | 11.12 | | |
| 18 | CSS | 2650 | 7.19 | 1699 | Na-Ca-SO4-Cl | 209.84 | 57.45 | 260.00 | 6.00 | 0.0 | 101.565 | 777 | 338.10 | 6.93 | -3.61 | -20.59 |
| 19 | F.B. | 2130 | 6.92 | 1371 | Na-Ca-SO4-Cl | 147.88 | 48.50 | 224.00 | 7.90 | 0.0 | 104.310 | 528 | 362.60 | 8.32 | -3.55 | -15.06 |
| 20 | F.B. | 2170 | 7.26 | 1322 | Na-Ca-SO4-Cl | 149.64 | 47.15 | 210.67 | 7.20 | 0.0 | 107.055 | 511 | 342.60 | 8.64 | -3.70 | -15.71 |
| 21 | F.B. | 1840 | 7.21 | 1134 | Na-Ca-SO4-Cl | 124.92 | 40.98 | 194.00 | 6.00 | 0.0 | 126.270 | 411 | 294.00 | 9.35 | | |
| 22 | F.B. | 4240 | 7.19 | 2383 | Ca-Na-Cl | 385.88 | 116.60 | 318.00 | 8.00 | 0.0 | 93.330 | 503 | 1004.50 | 9.03 | -2.32 | -11.08 |
| 23 | F.B. | 4090 | 6.75 | 2587 | Ca-Na-Cl-SO4 | 345.56 | 105.48 | 376.00 | 11.00 | 10.8 | 38.430 | 903 | 816.30 | 4.48 | | |
| 24 | F.B. | 2690 | 7.04 | 1785 | Ca-Na-Cl-SO4 | 238.20 | 76.96 | 247.00 | 6.30 | 0.0 | 115.290 | 503 | 655.50 | 10.58 | | |
| 25 | F.B. | 3700 | 6.75 | 2420 | Ca-Na-SO4-Cl | 335.48 | 110.60 | 310.00 | 8.80 | 0.0 | 109.800 | 939 | 661.50 | 9.81 | -3.24 | -14.54 |
| 26 | F.B. | 1420 | 7.20 | 934 | Na-Ca-SO4-Cl | 126.36 | 32.53 | 147.00 | 3.50 | 0.0 | 118.035 | 330 | 235.20 | 12.47 | -2.27 | -10.91 |
| 27 | F.B. | 1280 | 6.88 | 722 | Ca-Na-Cl | 115.69 | 25.24 | 114.00 | 3.20 | 0.0 | 120.780 | 173 | 230.30 | 10.39 | | |
| 28 | F.B. | 4200 | 6.62 | 2639 | Ca-Na-SO4-Cl | 371.84 | 69.95 | 414.00 | 6.90 | 10.8 | 32.940 | 1280 | 469.50 | 3.78 | 1.29 | 1.64 |
| 29 | F.B. | 1020 | 6.55 | 575 | Na-Ca-Cl-SO4 | 81.86 | 21.45 | 95.00 | 3.50 | 0.0 | 93.330 | 155 | 171.50 | 7.33 | | |
| 30 | F.B. | 940 | 7.25 | 533 | Ca-Na-Cl-SO4 | 94.67 | 19.70 | 70.40 | 3.50 | 0.0 | 96.075 | 140 | 157.00 | 8.16 | -3.53 | -15.80 |
| 31 | Rain | 120 | 8.73 | 74 | Na-HCO3 | 8.00 | 3.50 | 15.00 | 2.00 | 2.6 | 47.450 | 13 | 6.40 | 0.00 | -3.85 | -13.98 |
| 32 | Sea | 57800 | 8.10 | 41722 | Na-Cl | 392.00 | 1420.00 | 13400.00 | 397.00 | 25.0 | 176.900 | 3100 | 22900.00 | 0.62 | 1.34 | 9.58 |

**Note:** Q= Quaternary, CSS= Carboniferous Sandstone, FB= Fractured Basement

Ca-Na-$SO_4$-Cl and Na-Ca-$SO_4$-Cl types. Such water types reveal that sulphate ions predominate over chloride and bicarbonate ions in the majority of samples. In all cases, the bicarbonate ion did not exceed the sulfate or chloride ions in any of the samples.

The higher Ca and Na concentrations in the groundwater samples are indicative of the leaching and dissolution of the weathered granite rocks rich in plagioclase feldspar. The origin of calcium can be traced back to gabbro rock, which contains pyroxene and calcium-rich plagioclase. Meanwhile, sodium is sourced from diorite rock, which differs from gabbro due to the composition of the plagioclase species. Plagioclase in diorite is higher in sodium and lower in calcium (Robertson, 1999 and Philpotts and Ague, 2022).

Additionally, the dominance of $SO_4$ and Cl over $HCO_3$ might have multiple causes, including medium evolutionary stage of groundwater and/or dissolution of minerals rich in gypsum and anhydrite, in addition to an increased evaporation with low recharge rates. Although the TDS values in some samples of the fractured basement aquifer were less than 1000 mg/l (samples 18, 19, 21, 22), they followed the same sequence as all samples with regard to ion sequence. This can be explained by the fact that the wells from which these samples were taken are close to the watershed areas.

Water type can be also recognized using a graphical ternary diagram (Fig. 4).This graph is used to identify the chemical facies of water samples, particularly groundwater (Zaporozec, 1972). It is a useful tool for visualizing the chemical composition of water and determining the dominant ions and their relative proportions. By plotting water samples on the ternary diagram, it is obvious that all the Quaternary water points fall in the Na and $SO_4$ fields. As for the carboniferous aquifer, the majority of the samples are located in the Na and $SO_4$ fields, while a minority are located in the Ca and Cl fields. For the fractured basement aquifer, about 60% of the samples plot in the Na and $SO_4$ fields, while the remaining 40% plot in the Ca and Cl fields. Generally, groundwater is significantly dominated by Na and Ca over Mg and K and by strong acids ($SO_4$ + Cl) over weak acids ($CO_3$ + $HCO_3$). This may suggest that the water has passed through weathered rocks that contain minerals such as halite or gypsum, leading to an increase in sulfate and chloride ions.

Groundwater movement modifies the distribution of some ions and related ion ratios. Therefore, the relationships between ion ratios in groundwater can provide important information about the geochemical processes that have occurred in the aquifer. Scatter diagrams are one of the tools used to assess groundwater data, along with additional geochemical and hydrological information that should be taken into account when discussing groundwater chemistry (Hounslow, 2018). As a result, by comparing some ion species with other selected ionic ratios, it is possible to evaluate the chemical evolution trends of groundwater, identify the source of groundwater, assess the sources of chemical constituents, and give more explanation about the various geochemical processes that have impacted the groundwater.

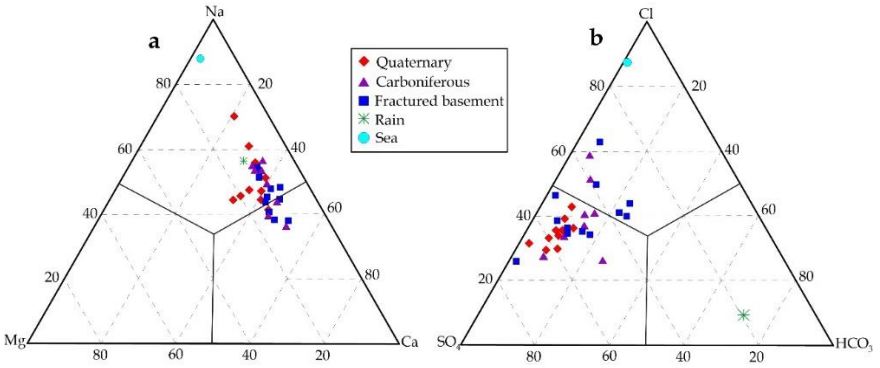


**Fig. (4).** Ternary diagrams comprising **a.** Mg, Na, Ca and **b.** $SO_4$, Cl and $HCO_3$ trilinears.

The relationships between some selected ion ratios that are thought to be of some significance in this regard include Na/Cl versus Ca/Mg, Mg/Ca+Mg vs. $HCO_3/SiO_2$, $HCO_3$+ $SO_4$ vs. Ca+Mg, and Ca/Ca+$SO_4$ vs. Na/Na+Cl (Fig. 5).

i- The Na/Cl versus Ca/Mg relationship diagram (Fig. 5a) is used to identify various processes occurred in groundwater (Hounslow, 2018). Based on the distribution of groundwater samples shown on this plot, it appears that certain Quaternary samples had undergone reverse ion exchange resulting in an increase of Mg and a decrease of Na, indicating the presence of groundwater with a longer residence time. Another group of samples, in partnership with the rest of the other samples, showed distinct geochemical processes such dissolution of calcite and dolomite, reverse ion exchange with an increase of Ca and a decrease of Na, and silicate weathering.

ii- The scatter plot of Mg/Ca+Mg vs. $HCO_3/SiO_2$ adopted by Hounslow (2018) (Fig. 5b) is used to determine the rock type with which water has interacted while flowing through pores and fractures. The scatter plot reveals that a majority of the samples were located in region 1A, indicating that their composition is primarily related to "not silicate weathering" and specifically related to the weathering of carbonate rocks, such as calcite-dolomite minerals. One sample from the quaternary alluvium aquifer, labeled as sample 2, was also linked to non-silicate rock weathering, but it falled in region 1B, demonstrating the influence of marine sediments. Additionally, three samples from the fractured basement aquifer were situated in the ambiguous area 1C. Two other samples, one from the fractured basement and the other from the carboniferous, were positioned on the line y = 5 ($HCO_3$ /$SiO_2$), indicating that factors other than silicate or carbonate weathering, such as cation exchange, influence the chemical composition of the water.

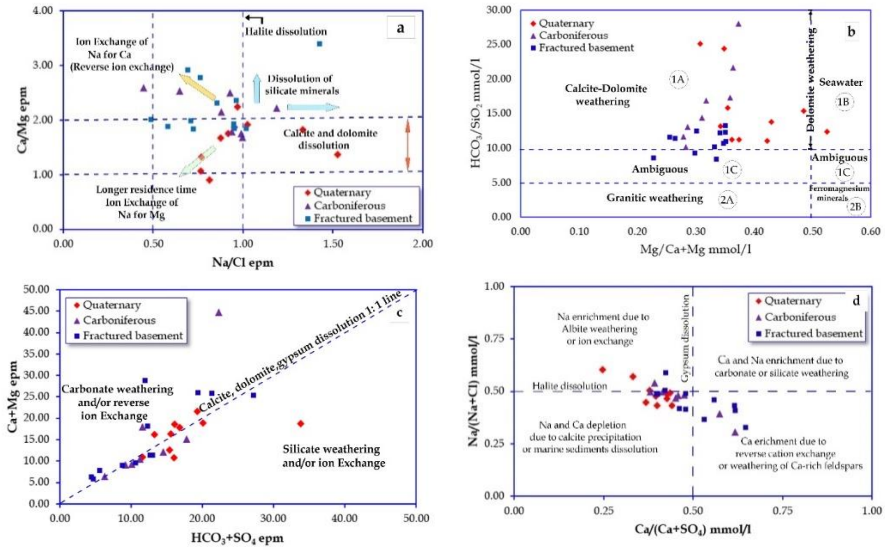


**Fig. (5).** Scatter diagrams with the principal cations and anions correlated to distinguish between the different geochemical processes.

iii- The Ca+Mg against $SO_4$+$HCO_3$ plot (Fig. 5c) demonstrates that the majority of the groundwater studied samples were found around the 1:1 line. The samples plotting above the line indicate that calcium and magnesium are being released into groundwater because of reverse ion and/or carbonate weathering. The samples distributed below the line, on the other hand, could be attributed to silicate weathering and/or direct ion exchange. This interpretation supports what has been perceived in Fig. (5b). The figure also shows that few samples plotting on the 1:1 line, suggesting calcite, and dolomite and gypsum dissolution.

iv- The scatter plot of Na/Na+Cl against Ca/Ca+$SO_4$ (Fig. 5d), along with the plots, can provide more explanation on the geochemical processes that control the chemical composition of groundwater. The location of the samples on upper left side of this plot suggests that groundwater has been subjected to silicate weathering (such as albite, $NaAlSi_3O_8$) and ion exchange, leading to an increase of Na ions. On the other hand, the depletion of Ca and Na ions in the other group of samples, located at the lower left part of the plot, suggests calcite precipitation and/or the impact of marine deposits. Some other samples situated in the lower right part of this plot suggest Ca ion enrichment due to reverse ion cation exchange and/or weathering of Ca-rich feldspars such as anorthite ($CaAl_2Si_2O_8$). This plot also indicates that there is no evidence of the enrichment of Ca and Na through carbonate or silicate weathering.

**1.2. Significant hydrochemical mechanisms**

Gibbs diagrams were created using the weight ratios of Na/(Na + Ca) and Cl/(Cl + $HCO_3$) vs TDS in mg/l (Fig. 6). This approach has been frequently utilized to assess the main chemical mechanisms affecting groundwater (hydrogeochemical processes), encompassing precipitation, rock-water interaction, and evaporation. The diagram is divided into three main parts: the lower right part, representing the influence of precipitation; the central part, indicating the dominance of the rock weathering process; and the upper right part, indicating the influence of evaporation. The location of the studied groundwater samples suggests that the rock-weathering process is the predominant factor influencing the geochemical evolution of most of the samples. The plot distribution of the samples reveals that nearly all the Quaternary samples, along with a substantial number of other samples from the other aquifers, had a Na/Na+Ca ratio greater than 0.5 and a high TDS level above 1000 mg/l. This suggests that not only groundwater is affected by rock weathering, but it is also influenced by the evaporation-crystallization process.

All the samples in the plot exhibit evolutionary paths that originate near the Ca or "rock source" end-member and undergo changes in composition as the groundwater flows and circulates within the aquifer matrix, eventually resulting in the Na-rich, high-salinity end-member. The alteration in composition and concentration along the flow path can be attributed to longer residence time of the groundwater as well as lower precipitation and/or runoff that enhances the evaporation process and leads to an increase in salinity. Additionally, the precipitation of $CaCO_3$ from solution causes an increase in the relative proportion of Na to Ca both in the tributaries and in the mainstream of the Wadi (Gibbs, 1970).

In general, this plot demonstrates that the main process influencing groundwater is the rock-water interaction, and it also addresses the impact of evaporation on groundwater chemistry.

**1.3. Chemical activity diagrams**

A chemical activity diagram is a graphical representation of the thermodynamic state of a chemical system, which can be used to interpret and understand the controls on groundwater chemistry in the Quaternary and Basement aquifers (Bethke 1994). The diagram shows the relationship between the activities of different chemical species in a solution, as well as the saturation state of the solution with respect to different minerals (Fig. 7). The chemical stability diagrams include fields for several crystalline minerals that can be used to forecast which minerals will react with groundwater, as well as the direction and extent of the reactions (Rogers, 1989). The activity diagram is created based on the log of the activity ratios of $Ca^+$, $Mg^+$, $Na^+$ or $K^+$ to $H^+$ versus the log of the activity of silicic acid ($H_4SiO_4$). The activities of the species involved in these diagrams were calculated using the PHREEQC 3.1.2 program (Parkhurst and Appelo, 2013).

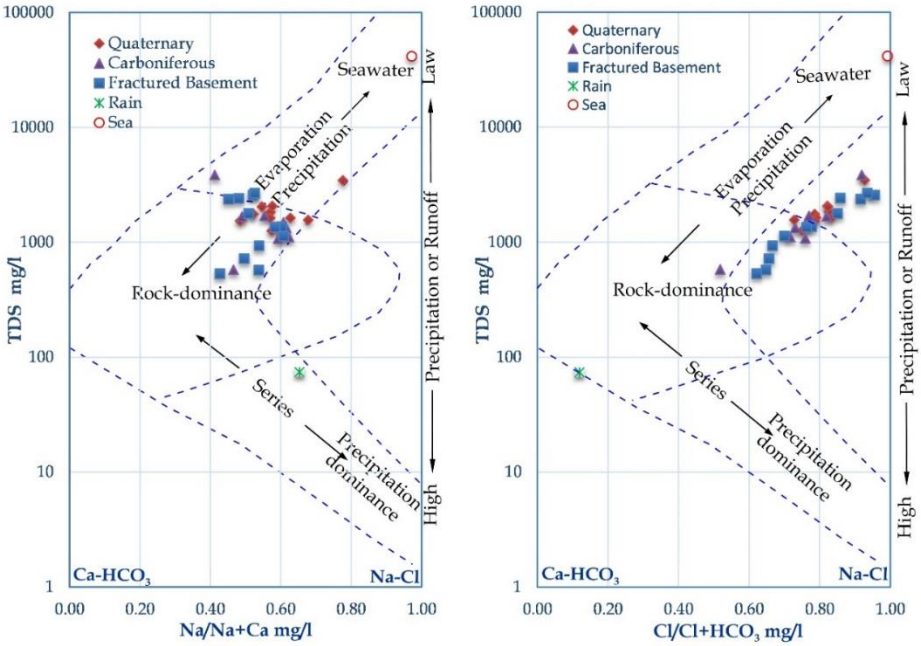


**Fig. (6).** Gibbs diagrams showing the main geochemical processes affected groundwater.

The mineral equilibria state of the studied groundwater samples indicates that the groundwater is in balance with the weathering byproduct of silicate minerals. Specifically, the minerals that are in equilibrium with the groundwater are kaolinite and gibbsite due to the interaction between rocks and water. Typically, kaolinite is frequently formed through the weathering of feldspar and other silicates (Garrels, 1967 and Nesbitt and Young, 1984).

Fig. (7a and b), which display the stability field diagrams of $Na^+$ and $Ca^+$ against silicic acid, reveal that the groundwater samples are positioned within the stability region of kaolinite and gibbsite. The $K^+$─ silicic acid stability diagram also shows similar results, with a few samples distributed in the illite field (Fig. 7c), indicating that illite is partially equilibrated with groundwater.

The position of the water points in these diagrams suggests that groundwater is mainly in equilibrium with kaolinite and gibbsite. Additionally, some water samples were located on the boundary between the stability fields of kaolinite and gibbsite, while a few samples plot close to the intersection of the saturation boundary of calcite in the $Ca^{2+}$─silicic acid stability diagram (Fig. 7b). The conclusion drawn from such diagrams are supported by the saturation indices calculated using the PHREEQC program, which shows positive values for the minerals kaolinite and gibbsite. However,

for illite, some samples had saturation indices that ranged from positive to negative values (Table 2).

In the basement rocks, the slope of the $\log Mg^{2+}/(H^+)^2$─$\log Na^+/H^+$ cross plot remained close to 2 until the log $Na^+/H^+$ value reached a maximum of approximately 5. After this point, the $\log Mg^{2+}/(H^+)^2$ value either remained constant or decreased, indicating that a mineral phase unique to the basement is limiting the concentration of $Mg^{2+}$ but not $Na^+$ in the groundwater (Barnes and Worden, 1998), (Fig. 7d). This observation can be explained by two hypotheses: either feldspars are undergoing chemical breakdown, releasing $Na^+$ and adsorbing $Mg^{2+}$ following the formation of smectite commonly found within the basement rocks, or cation exchange is occurring, with $Na^+$ replacing $Mg^{2+}$ at exchange sites on clay. In either case, the cation chemistry of the groundwater is likely controlled by cation exchange reactions involving alkali and alkali earth cations, as evidenced by the slopes of the $\log Mg^{2+}/(H^+)^2$─$\log Na^+/H^+$ cross plot (Krauskopf and Bird, 1979 and Smith and McAlister, 1995). The underlying substrate through which the groundwater flows contains an effectively infinite quantity of Na, Mg, and Ca, so increasing one of these components in the groundwater requires a corresponding alteration of the other components to maintain ionic balance.

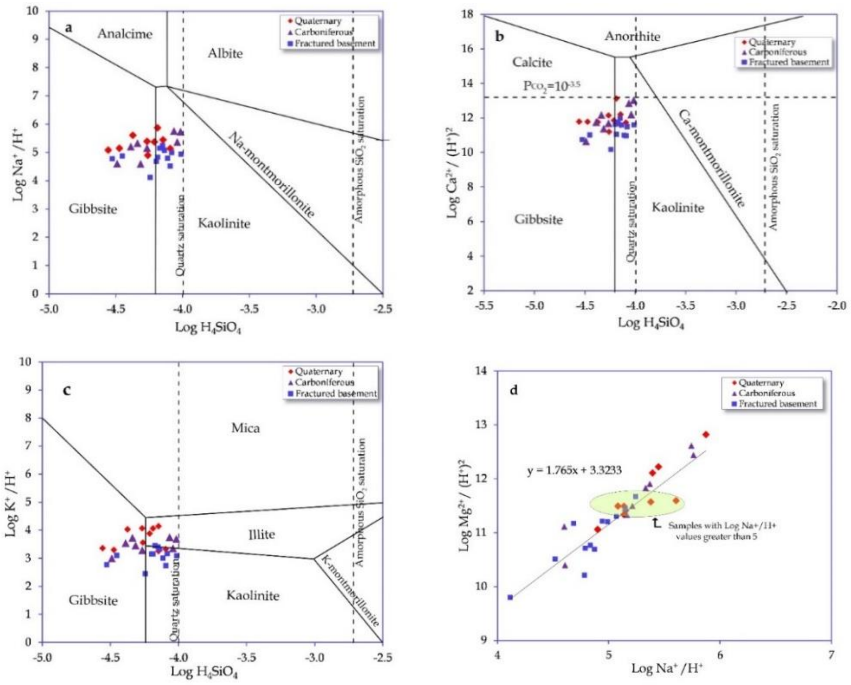


**Fig. (7).** Activity diagrams of **a.** Log $H_4SiO_4$ vs. Log $Na^+/H^+$; **b.** Log $H_4SiO_4$ vs. Log $K^+/H^+$; **c.** Log $H_4SiO_4$ vs. Log Ca+/$(H^+)^2$ and **d.** Log $Na^+/H^+$ vs. Log $Mg^{2+}/(H^+)^2$.

**Table (2).** Saturation states and their percent of some selected minerals for the studied groundwater samples.

| Mineral | Chemical formula | Saturation indices (SI) | | | Percent of SI (%) | |
|---|---|---|---|---|---|---|
| | | Min | Max | Mean | Undersaturated | Oversaturated |
| Albite | $NaAlSi_3O_8$ | -5.02 | -0.95 | -2.94 | 100 | 0 |
| Anhydrite | $CaSO_4$ | -1.73 | -0.58 | -1.11 | 100 | 0 |
| Anorthite | $CaAl_2Si_2O_8$ | -6.49 | -0.58 | -3.78 | 100 | 0 |
| Calcite | $CaCO_3$ | -1.10 | 0.59 | -0.23 | 77 | 23 |
| Dolomite | $CaMg(CO_3)_2$ | -2.45 | 0.90 | -0.63 | 80 | 20 |
| Gibbsite | $Al(OH)_3$ | 0.07 | 2.66 | 1.21 | 0 | 100 |
| Gypsum | $CaSO_4{:}2H_2O$ | -1.42 | -0.28 | -0.80 | 100 | 0 |
| Halite | NaCl | -6.66 | -4.98 | -5.68 | 100 | 0 |
| Illite | $K_{0.6}Mg_{0.25}Al_{2.3}Si_{3.5}O_{10}(OH)_2$ | -4.00 | 3.00 | -0.36 | 40 | 60 |
| Kaolinite | $Al_2Si_2O_5(OH)_4$ | -0.10 | 5.88 | 2.74 | 3 | 97 |
| Amorphous silica | $SiO_2$ | -1.84 | -1.30 | -1.52 | 100 | 0 |

### 1.4. Saturation indices and stability relations between water and rock

The results summarized in Table (2) represent the saturation indices of several minerals, which were calculated using the PHREEQC speciation program. The results indicate that most of the groundwater samples were oversaturated with respect to kaolinite ($Al_2Si_2O_5(OH)_4$) and gibbsite ($Al(OH)_3$), and around 60% of the samples were oversaturated with respect to illite ($K_{0.6}Mg_{0.25}Al_{2.3}Si_{3.5}O_{10}(OH)_2$ ). The results support the conversion of feldspars to kaolinite (Langmuir, 1997).

$$2NaAlSi_3O_8 + 2CO_2 + 11H_2O \rightarrow Al_2Si_2O_5(OH)_4 + 2Na^+ + 4H_4SiO_4 + 2HCO_3^- \quad (2)$$

$$2KAlSi_3O_8 + 2CO_2 + 11H_2O \rightarrow Al_2Si_2O_5(OH)_4 + 2K^+ + 4H_4SiO_4 + 2HCO_3^- \quad (3)$$

The relationship between pH and the partial pressure of $CO_2$ can provide further insights into the hypothesis. As depicted in Fig. (8), there is a negative correlation between the values of $Pco_2$ and pH, indicating that as pH values increase, the partial pressure of $CO_2$ decreases. This trend could be attributed to the longer residence time of groundwater in the aquifer, which allows for more chemical reactions with minerals in the aquifer. For example, feldspars can consume $CO_2$, leading to an increase in Na and $HCO_3$ concentrations and

potentially triggering the reactions described in equations 2 and 3. Consequently, the partial pressure of $CO_2$ decreases and the pH increases.

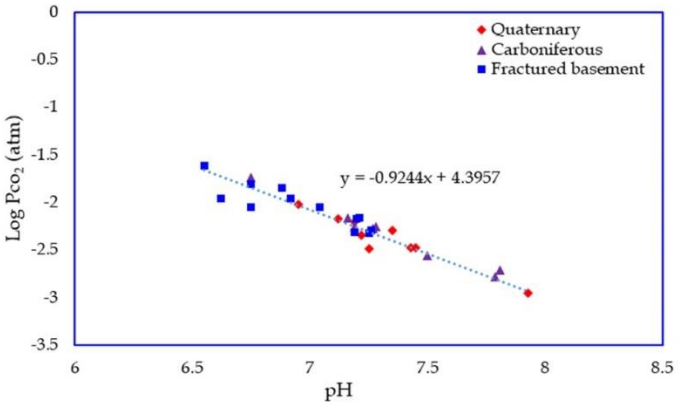


**Fig. (8).** The relationship between pH and log ($Pco_2$) for the studied groundwater.

The presence of groundwater in equilibrium with kaolinite, gibbsite, and partially equilibrated with illite, provides further support to the previous hypothesis proposed based on the chemical activity diagrams. Furthermore, the samples were undersaturated with albite ($NaAlSi_3O_8$), anhydrite ($CaSO_4$), anorthite ($CaAl_2Si_2O_8$), gypsum ($CaSO_4{:}2H_2O$), halite (NaCl), and amorphous silica ($SiO_2$), suggesting the influence of aluminosilicate minerals in the aquifer strata, which consist of shales and clays.

The correlation between Na and Cl and the saturation index of halite, as well as between Ca and $SO_4$ and the saturation index of gypsum, is illustrated in Fig. (9a and b). The dissolution of halite and gypsum can lead to exponential increases in Na, Cl, Ca, and $SO_4$ concentrations, indicating their impact on the groundwater chemistry during its circulation in the aquifer matrix. The saturation state analysis reveals that the majority of the groundwater samples were undersaturated with respect to calcite and dolomite, with about 77 and 80% of samples, respectively.

According to Langmuir (1971), a solution is considered to be saturated (or in equilibrium) with calcite if the saturation index is within +0.1 (Fig. 9c). Higher or lower values are indicative of water that is over or under-saturated with calcite, respectively (Cardenal et al., 1994).

The lack of correlation between the concentrations of Ca, $HCO_3$, Mg, and $HCO_3$ and the saturation indices of calcite and dolomite, as shown in Fig. (9c and d) suggest that the weathering of these minerals did not continue and only a portion of them were dissolving along the groundwater flow direction. This could be due to several factors, such as the inadequacy of calcium carbonate minerals in the aquifer material or chemical reactions that have

removed calcium and carbonate ions from the groundwater (Cardenal et al., 1994 and Appelo and Postma, 2004). As a result, the deficit of Ca ions is likely being compensated for by the dissolution of the matrix that is cemented within the aquifer material or by ion exchange reactions occurring on clay intercalations. This finding supports the hypothesis proposed in the hydrochemical coefficient section (section 4.1.1), which suggests that reverse ion exchange is a potential source of Ca and Mg ions in groundwater.

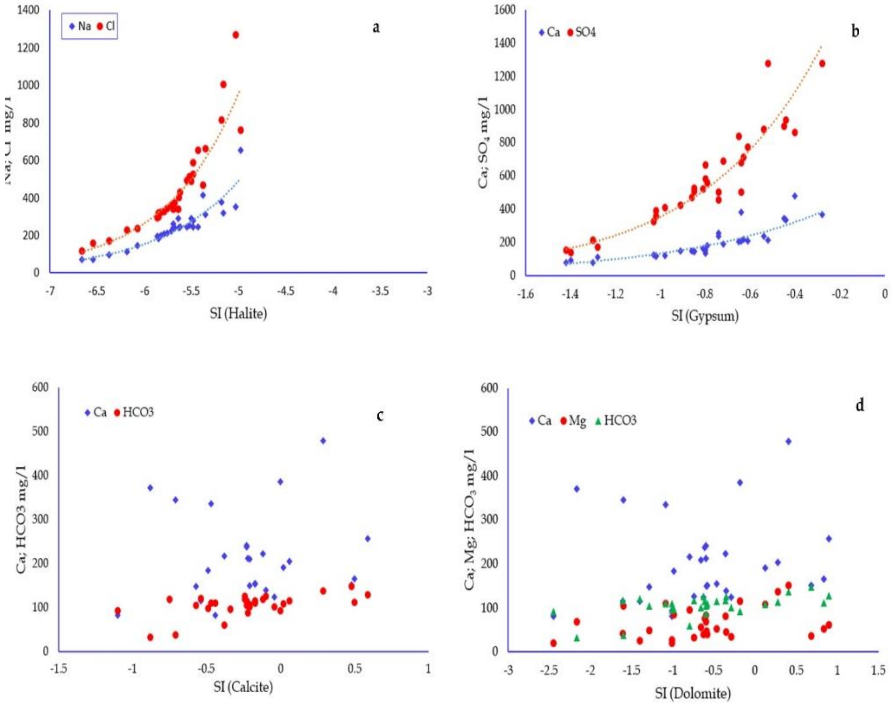


**Fig. (9).** Saturation indices scatter plots of some minerals with their corresponding ions.

**2. Stable Isotopes ($\delta^{18}O$ and $\delta^{2}H$)**

The groundwater samples that were studied exhibit a variable range of stable isotope compositions. Specifically, the $\delta^{18}O$ values vary from -4.28 to 2.32‰ and the $\delta^{2}H$ values vary from -20.17 to 8.27‰. In the Quaternary alluvium aquifer, the $\delta^{18}O$ and $\delta^{2}H$ values ranging from -3.80 to 2.32‰ and from -20.17 to 8.27‰, respectively. The Carboniferous aquifer displays $\delta^{18}O$ values ranging from -4.28 to -3.28‰ and $\delta^{2}H$ values ranging from -20.59 to -15.95‰. The fractured Precambrian basement aquifer exhibits $\delta^{18}O$ values ranging from -3.70 to 1.29‰ and $\delta^{2}H$ values ranging from -15.80 to 1.64‰.

The scatter plot of oxygen-18 against deuterium (Fig. 10a) reveals that almost all the samples cluster around the rainwater sample toward the

negative pole of the Global Meteoric Water Line (GMWL), which was proposed by Craig (1961). Few samples exhibited a linear regression line with the equation ($\delta^2H = 4.39O^{18} - 1.654$), indicating a relatively high slope, which suggests a continuous process of evaporation and/or dissolution enrichment.

The similarity in the isotopic composition ($\delta^{18}O/\delta^2H$) of groundwater across the studied aquifers indicates a common source of recharge, while slight variations in the samples of different aquifers and within the same aquifer indicate diverse hydrogeochemical processes. Groundwater with more depleted values could indicate a mixing between rainwater recharge and deep mineralized groundwater. Additionally, Fig. (10a) demonstrates also that seawater encroachment did not affect any of the groundwater studied samples.

To understand the groundwater processes, a bivariate plot was created to analyze the variation of δ18O‰ composition with TDS. Fig. (10b) indicates that a significant group of samples exhibited a relatively unchanged stable isotopic content with an increase of the TDS, indicating the occurrence of leaching and dissolution processes. A minor group was impacted by evaporation, resulting in an increase in isotopic content as the TDS increased.

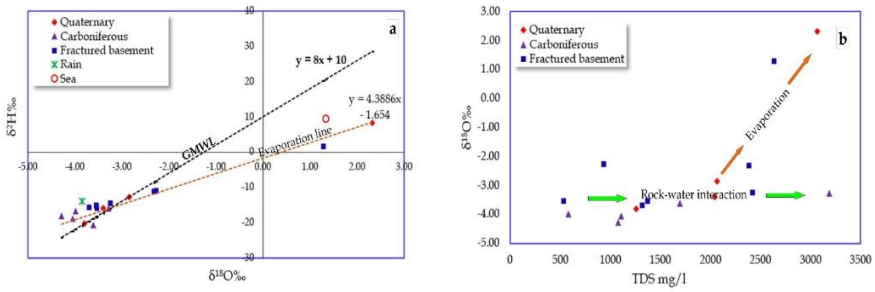


**Fig. (10).** (a) plot of $\delta^{18}O‰$ vs. $\delta^2H‰$ ; (b) plot of TDS vs. $\delta^{18}O‰$.

## 3. Factor Analysis

Factor analysis provides a significant advantage in hydrochemical interpretation as it is not influenced by the quantity or nature of variables utilized. Additionally, factor analysis yields comparable or even greater insights than visual tools, like trilinear diagrams, in terms of identifying water masses based on their factor classification. Factor analysis is a technique that is not limited by the number or nature of variables, and it treats each variable as an independent entity (Dalton and Upchurch, 1978). The primary aim of factor analysis is to decrease a vast array of variables into a condensed set of variables, which are known as factors. By using factor analysis method, the eigen values and factor loadings of the correlation matrix were determined, and the extraction factors were generated using the variances and covariances of the used variables.

Through the application of factor analysis on 12 variables, three distinct trends (factors) were identified, which collectively explain

approximately 86.14% of the total variability observed in the data. Table (3) presents the loadings of each variable on each factor and the percentage of total variability attributed to each variable as determined by the analysis.

**Table (3).** Rotated component matrix.

| Variables | Component | | |
|---|---|---|---|
| | **I** | **II** | **III** |
| pH | -0.06 | -0.22 | 0.87 |
| TDS | 0.88 | 0.45 | -0.02 |
| Ca | 0.93 | 0.10 | -0.28 |
| Mg | 0.93 | 0.10 | 0.21 |
| Na | 0.60 | 0.75 | 0.07 |
| K | 0.19 | 0.67 | 0.61 |
| $HCO_3$ | 0.09 | -0.87 | 0.41 |
| $SO_4$ | 0.62 | 0.68 | -0.12 |
| Cl | 0.95 | 0.07 | 0.09 |
| $SiO_2$ | 0.48 | -0.53 | 0.26 |
| $\delta^{18}O‰$ | 0.25 | 0.92 | -0.04 |
| $\delta D‰$ | 0.23 | 0.90 | 0.03 |
| Total eign value | 6.26 | 2.80 | 1.37 |
| Total variance % | 52.14 | 23.32 | 11.42 |
| Cumulative % | 52.14 | 75.46 | 86.88 |

Extraction Method: Principal Component Analysis. Rotation Method: Varimax with Kaiser Normalization.

Factor I displayed a highly positive correlation with TDS, Ca, Mg, Cl, and a moderately positive correlation with Na, $SO_4$, and $SiO_2$. The strong positive correlation with TDS suggests that this factor is an indicator of the overall mineralization of the groundwater. The high positive correlations with Ca, Mg, and Cl as well as the moderate positive loading with $SO_4$ suggest the impact of the reverse ion exchange and the dissolution of the evaporite minerals, such as gypsum and halite. The moderate positive correlation with Na, and $SiO_2$, suggests that silicate weathering may also be contributing to the observed trends in Factor I.

Factor II displayed a strong positive association with $\delta^{18}O$ and $\delta D‰$, as well as a significant negative correlation with $HCO_3$. It indicates also a moderate positive correlation with TDS, K, and $SO_4$, and a moderate negative correlation with $SiO_2$. This factor also highlights the role of the rock-water interaction processes, including direct ion exchange and evaporation in shaping the groundwater chemistry.

Factor III was a weaker factor, characterized by a strong positive association with pH and a moderate positive correlation with K and $HCO_3$. This factor is likely associated with the weathering of feldspars, as well as the flushing of carbonate-bearing minerals due to the interaction of carbonic acid-

rich rainwater with the weathering products of the surrounding igneous and carbonate rocks.

## 4. Recharge Rate Estimation to Groundwater in Wadi Sidri Area

The chloride mass balance (CMB) method is a widely used approach for estimating groundwater recharge rates. The application of the CMB is based on the knowledge of annual precipitation and Cl concentrations in rainfall as well as in groundwater storage (Scanlon et al., 2002). Because of its conservative nature, chloride is a particularly instructive ion in hydrochemistry. As a result, CMB techniques are widely utilized to predict recharge rates in both saturated and unsaturated zones (Sharma and Hughes, 1985; Varni et al., 1999 and Tweed et al., 2011).

In this study, the CMB method, adopted by Eriksson (1976), is used. This method relies on the assumption that the chloride concentration in precipitation remains constant over time and that all chloride in the groundwater is derived solely from precipitation. The absence of evaporites in the study area makes it unlikely that the weathering of host rocks has led to a noteworthy increase in chloride content. Therefore, any increase in chloride concentration in groundwater above that in precipitation is assumed to be the result of evaporation from rainfall. Furthermore, chloride does not participate, adsorbed or exchanged, in any chemical reactions during water movement.

Based on these assumptions, the groundwater recharge rate can be estimated as follows:

$$R = \frac{(V_o \; x \; C_o)}{(C)} \qquad (3)$$

Where,

R is the annual recharge (mm/y).

$V_o$ is the annual mean precipitation (mm/y) within eight hydrologic years (1981-2021, DRC stations).

$C_o$ is the initial mean concentration of chloride in rainwater.

C is the harmonic mean of chloride concentrations in groundwater.

To apply the CMB method as presented in Equation (3), mean yearly rainfall records (1981–2021) were obtained from the Global Weather Data for SWAT web site (CFSR). The mean chloride concentration in rainwater was initially determined using two samples taken during the winter of 2020. One sample was collected near the outlet of Wadi Sidri, close to the Gulf of Suez, and had a chloride concentration of 12.25 mg/l. The other sample was taken about 15 km away from the gulf and had a chloride concentration of 6.4 mg/l. The average of these two concentrations was calculated to be 9.33 mg/l, which was used as the initial mean chloride concentration in rainwater. Equation (3) employs harmonic means because they are intermediate between arithmetic and geometric means in terms of the values they produce. As a result, they are considered more representative than either of the other two means.

The results presented in Table (4) show that the annual recharge rates (R) for the Quaternary, Carboniferous and fractured basement aquifers are 0.48, 0.66 and 0.64 mm/y, respectively. The overall estimate of the recharge for the whole areas was 1.78 mm/y for 1981 to 2021 period. The results show also that the recharge in these aquifers represented 2.18, 2.99 and 2.90% of annual rainfall for the Quaternary, Carboniferous and fractured basement aquifers, respectively with a total percentage of 8.06%. To verify the accuracy of the approach, the recharge rate percentage estimated in this study (8.06%) was applied to the total amount of rainfall on Wadi Sidri basin ($53.4 \times 10^6$ $m^3$), as previously calculated by Masoud (2011). This resulted in a net recharge to the groundwater of $4.3 \times 10^6$ $m^3/y$. This value was then compared to the amount of rainfall recharged to groundwater in Wadi Sidri, which was determined to be $5.99 \times 10^6$ $m^3/y$ by Elewa and Qaddah (2011). The difference in both calculations could possibly identify another source of chloride to groundwaters aside from rainfall. Direct evaporation from the shallow water table and the weathering of marine sediments from the nearby El-Tih Plateau may also contribute to the presence of chloride in the groundwater. This implies that the CMB method can be used as a complementary method with the other hydrologic methods in the estimation of the rainfall recharge to groundwaters.

**Table (1).** Calculation of recharge rate of the different aquifers according to Eriksson (1975).

| Aquifer | AMP (mm/y) ($V_o$) | IMC of chloride in rainwater (mg/l) ($C_o$) | HMC of chloride in groundwater (mg/l) (C) | Annual recharge (mm/y) (R) | Recharge rate (R%) |
|---|---|---|---|---|---|
| Quaternary | 22.05 | 9.33 | 427.01 | 0.48 | 2.18 |
| Carboniferous | 22.05 | 9.33 | 312.33 | 0.66 | 2.99 |
| Fractured Basement | 22.05 | 9.33 | 322.06 | 0.64 | 2.90 |
| All studied aquifers | 22.05 | 9.33 | 347.66 | 1.78 | 8.06 |

*Note : (AMP) = annual mean precipitation, (IMC) = initial mean concentration, (HMC) = harmonic mean concentration.

## CONCLUSIONS

Wadi Sidri represents one of the main Wadis in South Sinai of Egypt. The presence of groundwater in the Wadi Sidri basin is influenced by several factors, including the fluctuation of the bedrock surface, the meandering shape of the main drainage channel, and the fractured bounding scarps that affect the downstream movement of groundwater. Rainfall represents the main source of water supply and groundwater is exploited from various aquifers, including Quaternary alluvium, the Carboniferous sandstone, and the fractured Precambrian basement. The heterogeneity of the groundwater chemical

composition, even in the same aquifer, reflects different processes such as precipitation, evaporation and dissolution of the minerals interbedded within the aquifer material as well as distance from the watersheds.

The groundwater in the studied aquifers is dominated by the Ca-Na-$SO_4$-Cl and Na-Ca-$SO_4$-Cl water types, reflecting medium evolutionary stage of groundwater. The relationships between some selected ion ratios as well as stable isotopes indicate that rock-water interaction is the dominant process. Rock-water interactions occur through multiple hydrogeochemical processes including reverse and direct ion exchange, as well as silicate and carbonate weathering. The chemical activity diagrams, saturation indices calculations, and the relationship between pH and log$Pco_2$ indicate that some minerals such as kaolinite, gibbsite, and illite are in equilibrium with the groundwater due to silicate weathering and cation exchange. This leads to an increase in Na and Ca concentration and a decrease in Mg concentration in the water. Scatter plots of certain ionic ratios, such as Mg/Ca+Mg vs. $HCO_3/SiO_2$ and $HCO_3$+ $SO_4$ vs. Ca+Mg, suggest carbonate weathering. Saturation index calculations support this conclusion, with calcite and dolomite being found to be undersaturated in the solution. The SPSS program identifies three factors that impact groundwater chemistry, including leaching and dissolution, silicate and carbonate weathering, and the impact of marine minerals interbedded in the aquifer matrix.

Finally, the application of the CMB method indicates that about 8.06% of rainwater seeps into groundwater, corresponding to 4.3 $x10^6$ $m^3/y$. Therefore, evaluating the recharge rate of precipitation into groundwater and monitoring its chemical composition is crucial for sustainable development and establishing new communities in arid and semiarid environments.

## ACKNOWLEDGEMENT

The author is greatly indebted to Prof. M.K. Sallouma for his valuable comments and suggestions that enriched this manuscript.

## REFERENCES

Afandy, A., M. Geriesh, S. Eweda, A. Alshami and K. Halim (2016). Hyrogeochemisrty and radioactivity of groundwater in Baba- Sidri basins, Southwest Sinai, Egypt. Bulletin of Faculty of Science, Zagazig University, 38: 32.

Aggour, T. and M. Gomaa (2008). Hydrogeological and hydrogeochemical studies in Wadi Baba and Sidri, Southwestern part of Sinai. Egypt Annals Geol. Surv. Egypt, 30: 497-528.

Aglan, O. (1995). Geology of groundwater supplies in the area between Wadi Gharandal and Wadi Sidri, Southwestern Sinai. Msc. Thesis, Geol. Dept., Fac. Sci., Ain Shams Univ., Egypt, 202 p.

Allison, G. and M. Hughes (1978). The use of environmental chloride and tritium to estimate total recharge to an unconfined aquifer. Soil Research, 16: 181-195.

Appelo, C.A.J. and D. Postma. (2004). In: 'Geochemistry, Groundwater and Pollution'. CRC press.

Arnous, M.O. and A.E. Omar (2018). Hydrometeorological hazards assessment of some basins in Southwestern Sinai area, Egypt. Journal of Coastal Conservation, 22: 721-743.

Barnes, S. and R. Worden (1998). Understanding groundwater sources and movement using water chemistry and tracers in a low matrix permeability terrain: the Cretaceous (Chalk) Ulster White Limestone Formation, Northern Ireland. Applied Geochemistry, 13: 143-153.

Bethke, C. (1994). In: 'The Geochemist's Workbench'. Version 2.0: A Users Guide to Rxn, Act2, Tact, React, and Gtplot, 213 p.

Cardenal, J., J. Benavente and J. Cruz-Sanjulian (1994). Chemical evolution of groundwater in Triassic gypsum-bearing carbonate aquifers (Las Alpujarras, Southern Spain). Journal of Hydrology, 161: 3-30.

Conoco, C. (1987). Geological map of Egypt, scale 1: 500,000-NF 36 NE-Bernice, Egypt. The Egyptian General Petroleum Corporation, Cairo.

Cook, P.G. (2003). In: 'A Guide to Regional Groundwater Flow in Fractured Rock Aquifers'. Henley Beach, South Australia: Seaview Press. Citeseer, 151 p.

Craig, H. (1961). Isotopic variations in meteoric waters. Science, 133: 1702-1703.

Dalton, M.G. and S.B. Upchurch (1978). Interpretation of hydrochemical facies by factor analysis. Groundwater, 16: 228-233.

De Vries, J.J. and I. Simmers (2002). Groundwater recharge: an overview of processes and challenges. Hydrogeology Journal, 10: 5-17.

Edmunds, W. and C. Gaye (1994). Estimating the spatial variability of groundwater recharge in the Sahel using chloride. Journal of Hydrology, 156: 47-59.

El Aref, M. (1988). On the geology of the basement rocks, East of Abu Zenima, West Central Sinai, Egypt. Egypt. J. Geol., 32: 1-25.

Elewa, H.H. and A.A. Qaddah (2011). Groundwater potentiality mapping in the Sinai Peninsula, Egypt, using remote sensing and GIS-watershed-based modeling. Hydrogeology Journal, 19: 613-628.

Eriksson, E. (1976). The Distribution of Salinity in Groundwater of the Delhi Region and the Recharge Rates of Groundwater. In: 'Interpretation of Environmental Isotopes and Hydrochemical Data in Groundwater Hydrology'. IAEA, Vienna, pp. 171–177.

Eriksson, E. and V. Khunakasem (1969). Chloride concentration in groundwater, recharge rate and rate of deposition of chloride in the Israel Coastal Plain. Journal of Hydrology, 7: 178-197.

Fishman, M.J. and L.C. Friedman (1989). In: 'Methods for Determination of Inorganic Substances in Water and Fluvial Sediments'. US Department of the Interior, Geological Survey. Book 5, Chapter A1.

Foster, S., A. Bath, J. Farr and W. Lewis (1982). The likelihood of active groundwater recharge in the Botswana Kalahari. Journal of Hydrology, 55: 113-136.

Garrels, R.M. (1967). Genesis of some ground waters from igneous rocks. Researches in Geochemistry, 2: 405-420.

Gibbs, R.J. (1970). Mechanisms controlling world water chemistry. Science, 170: 1088-1090.

Hammad, F. and R. Misak (1985). Quantitative geomorphology and groundwater possibilities in the vicinities of Wadi Nasib, Abu Zeneima, Sinai, Egypt. Desert Institute Bulletin, 35: 331-351.

Hiscock, K. (2005). Hydrogeology–Principles and Practice. Blackwell Science Ltd. London, UK.

Hounslow, A. (2018). In: 'Water Quality Data: Analysis and Interpretation'. CRC press, 416 p.

Kapos, V., J. Rhind, M. Edwards, M. Price and C. Ravilious (2000). Developing a map of the world's mountain forests. In: 'Forests in Sustainable Mountain Development: a State of Knowledge Report for 2000. Task Force on Forests in Sustainable Mountain Development, Cabi Publishing Wallingford, UK, pp. 4-19.

Krauskopf, K. and D. Bird (1979). In: 'Introduction to Geochemistry'. McGraw-Hill, New York, 617 p.

Langmuir, D. (1971). The geochemistry of some carbonate ground waters in central Pennsylvania. Geochimica et Cosmochimica Acta, 35: 1023-1045.

Langmuir, D. (1997). In: 'Aqueous Environmental Geochemistry'. Englewood Cliffs, NJ: Prentice-Hall, Inc., 601 p.

Lerner, D.N. (2020). Groundwater Recharge. In: 'Geochemical Processes, Weathering and Groundwater Recharge in Catchments'. CRC Press, pp.109-150.

Masoud, A.A. (2011). Runoff modeling of the wadi systems for estimating flash flood and groundwater recharge potential in Southern Sinai, Egypt. Arabian Journal of Geosciences, 4: 785-801.

Nesbitt, H.W. and G.M. Young (1984). Prediction of some weathering trends of plutonic and volcanic rocks based on thermodynamic and kinetic considerations. Geochimica et Cosmochimica Acta, 48: 1523-1534.

Parkhurst, D. and C. Appelo (2013). PHREEQC (Version 3)-A Computer Program for Speciation. Batch-Reaction, One-Dimensional

Transport, and Inverse Geochemical Calculations. Denver, Colorado, US Geological Survey, Water Resources Division, USA.

Philpotts, A.R. and J.J. Ague (2022). In: 'Principles of Igneous and Metamorphic Petrology'. Cambridge University Press, 26 p.

Rice, E.W., L. Bridgewater and A.P.H. Association (2012). In: 'Standard Methods for the Examination of Water and Wastewater'. American Public Health Association, Washington, DC, 724 p.

Robertson, S. (1999). British Geologic Survey, Rock Classification Scheme (Vol. 2). In: 'Classification of Metamorphic Rocks'. Keyworth, RR/99/002.

Rogers, R.J. (1989). Geochemical comparison of ground water in areas of New England, New York, and Pennsylvania. Groundwater, 27: 690-712.

Saad, K. F., El Shamy, I. Z. and Sewidan, A. S. (1980). Quantitative analysis of the geomorphology and hydrology of Sinai Peninsula: Ann. Geol. Surv. Egypt, X, 819-836.

Scanlon, B.R., R.W. Healy and P.G. Cook (2002). Choosing appropriate techniques for quantifying groundwater recharge. Hydrogeology Journal, 10: 18-39.

Sharma, M. and M. Hughes (1985). Groundwater recharge estimation using chloride, deuterium and oxygen-18 profiles in the deep coastal sands of Western Australia. Journal of Hydrology, 81: 93-109.

Shata, A. (1955). Some remarks on the distribution of the Carboniferous Formations in Egypt. Bulletin de l'Institut du Désert d'Egypte, 5: 241-247.

Smith, B. and J. McAlister (1995). Mineralogy, chemistry and palaeoenvironmental significance of an Early Tertiary Terra Rossa from Northern Ireland: A preliminary review. Geomorphology, 12: 63-73.

Tweed, S., M. Leblanc, I. Cartwright, G. Favreau and C. Leduc (2011). Arid zone groundwater recharge and salinization processes; an example from the Lake Eyre Basin, Australia. Journal of Hydrology, 408: 257-275.

Varni, M., E. Usunoff, P. Weinzettel and R. Rivas (1999). Groundwater recharge in the Azul aquifer, central Buenos Aires province, Argentina. Physics and Chemistry of the Earth, Part B: Hydrology, Oceans and Atmosphere, 24: 349-352.

Zaporozec, A. (1972). Graphical interpretation of water-quality data. Groundwater, 10: 32-43.

# العمليات الجيوكيميائية المؤثرة على نوعية المياه الجوفية بحوض وادي سدري، جنوب سيناء، مصر

**هشام عبد الحميد عز الدين**
قسم الهيدروجيوكيمياء، مركز بحوث الصحراء، القاهرة، مصر

تتأثر كيميائية المياه الجوفية في البيئات القاحلة وشبه القاحلة عادة بمجموعة من العمليات الهيدروجيوكيميائية المختلفة، بما في ذلك كمية الأمطار الساقطة، والتفاعل بين الماء والصخور، وكذلك التبخر. لذلك كان من الضروري تقييم كمية ونوعية المياه التي يتم شحنها إلى الخزانات الجوفية بدقة، وذلك للوقوف على مدى استدامة هذه المياه وصلاحيتها للاستخدام في الأغراض المختلفة مثل الأنشطة المنزلية والزراعية. اعتمدت هذه الدراسة على استخدام بعض الأشكال التوضيحية التقليدية مثل الشكل الثلاثي وشكل جبس، وكذلك على تحليل الارتباط بين المعاملات المختلفة لفهم العمليات الهيدروكيميائية التي أثرت على كيميائية المياه الجوفية في حوض وادي سدري، بسيناء، مصر. كما شملت الدراسة أيضًا على استخدام طريقة توازن كتلة الكلوريد (CMB) لحساب كمية الأمطار التي تغذي الخزانات الجوفية. أظهر الشكل ثلاثي الأبعاد (Ternary diagram) هيمنة عنصري Na، Ca على كلًا من K، Mg في حين تهيمن شقوق الأحماض القوية ($SO_4$+Cl) على شقوق الأحماض الضعيفة ($CO_3$+$HCO_3$). كشف مخطط جيبس أن تفاعل الماء مع الصخور هو العامل الرئيسي المؤثر على كيمياء المياه الجوفية، كما أشار أيضًا إلى تأثير عامل البخر في بعض العينات. أوضحت الارتباطات الأيونية بين نسبة أيونات متعددة مختارة، بما في ذلك (Na/Cl)–(Ca/Mg)، (Mg/Ca+Mg)–($HCO_3$/$SiO_2$)، (Na/Cl)–(Na/Na+Cl)، (Ca/Ca+$SO_4$)–($HCO_3$+$SO_4$)–(Ca+Mg)، أن عمليات التفاعل بين الصخور والمياه انطوت على آليات مختلفة أثرت في كيميائية المياه الجوفية، مثل التبادل الأيوني المنعكس والمباشر، بالإضافة إلى عمليات تجوية معادن السيليكات والكربونات وكذلك عمليات الغسيل والإذابة للرواسب البحرية المتداخلة في طبقات الخزان الجوفي. كشفت الأشكال الخاصة بالنشاط الكيميائي (chemical activity diagrams) لبعض العناصر مثل Ca, Mg, K, $H_2$ and Si أن عمليات تبادل الكاتيونات التي تنطوي على زيادة Na على حساب Mg قد أثرت على كيمياء المياه الجوفية. كما أشارت هذه الأشكال، جنبًا إلى جنب مع مؤشرات التشبع (SI) التي تم حسابها من خلال برنامج PHREEQC، إلى أن المياه الجوفية تتواجد في حالة اتزان كيميائي مع معادن الكاولينيت والجبسيت (kaolinite and gibbsite)، كما تتزن جزئيًا مع معدن الإليت (illite). أخيرًا تم استخدام طريقة توازن كتلة الكلوريد (CMB) لتقدير كمية مياه الأمطار المتسربة إلى الخزانات الجوفية، حيث أوضحت أن معدل تساقط كمية الأمطار على منطقة الدراسة هي ١.٧٨ مم/سنة للفترة من ١٩٨١ إلى ٢٠٢١، وأن النسبة التي تغذي المياه الجوفية تمثل حوالي ٨.٠٦٪ من إجمالي كمية الأمطار المتساقطة على منطقة الدراسة.